ENSO-Related Variability of the Southern Hemisphere Winter Storm Track over the Eastern Pacific–Atlantic Sector

SILVINA A. SOLMAN

Centro de Investigaciones del Mar y la Atmósfera, CONICET/UBA, and Departmento de Ciencias de la Atmósfera y los Océanos, Universidad de Buenos Aires, Buenos Aires, Argentina

CLAUDIO G. MENÉNDEZ

Centro de Investigaciones del Mar y la Atmósfera, CONICET/UBA, Buenos Aires, Argentina

(Manuscript received 25 January 2001, in final form 7 November 2001)

ABSTRACT

The interannual variability associated with the ENSO of winter storm tracks over the region extending from the eastern South Pacific Ocean across South America to the South Atlantic Ocean is described using 39 yr of data from the NCEP reanalysis data base. Tropical sea surface temperature anomalies associated with ENSO induce large-scale atmospheric circulation anomalies over large areas of the Southern Hemisphere. In particular, positive height anomalies dominate the Bellingshausen Sea during warm events, and consistently, a weakening of the eddy activity at low levels is found to the west of the Antarctic Peninsula. During El Niño (EN) the storm track evidences an equatorward shift over the subtropical Pacific Ocean and a slight strengthening in the central Atlantic Ocean.

Time-lagged correlation analysis applied to anomalies of the 300-hPa meridional wind at selected base points was used to study the structure and propagation characteristics of the waves. During EN, waves emanating from the Atlantic–Indian Ocean storm tracks tend to propagate preferably along the subpolar branch of the Pacific Ocean storm track near Australia. Over the subtropical Pacific Ocean the wave train propagates along a northern path compared with cold events consistent with an equatorward shift of the axis of maximum baroclinicity. Additionally, large eddy activity at lower levels but weak eddy activity at upper levels were found for that region. During La Niña (LN), wave packets propagate more coherently along the subtropical branch of the storm track over the South Pacific Ocean, attaining larger amplitudes at upper levels and developing over broader latitudes compared to the warm phase. A poleward deflection of subtropical waves and northeastward deflection of subpolar waves are also found for LN. Waves propagating through the Atlantic Ocean storm track evolve from the subtropical branch of the Pacific Ocean storm track for LN winters and from both the subtropical jet and the subpolar latitudes for EN.

1. Introduction

The storm tracks (i.e., areas where eddy activity is the strongest) are a rich phenomena directly or indirectly linked to virtually all aspects of large-scale atmospheric dynamics, playing a role in everything from daily weather to regional climate and climate variability. The patterns of interannual variability modulate this synoptic-scale activity mainly through changes in the basic state where waves are embedded. The variability of observed middle-latitude storm tracks in relation to low-frequency changes in the circulation pattern for the Northern Hemisphere winter has been vastly examined. In particular, the interannual variability associated with the El Niño–Southern Oscillation (ENSO) cycle includes differences in the shape and intensity of the North Pacific storm track (Lau 1985; Held et al. 1989; Orlanski 1998).

The Southern Hemisphere (SH) atmospheric circulation exhibits significant patterns of interannual to interdecadal timescales (e.g., Garreaud and Battisti 1999; Vera 2002). The storm tracks could influence, and be influenced by, the atmospheric long waves and in particular by their amplitude and location around the hemisphere. For example, an important signature related to ENSO events is the predisposition toward blocking southwest of the southern tip of South America during warm events, and vice versa during cold events (Rutllant and Fuenzalida 1991). This blocking anticyclone, frequently located around the Bellingshausen Sea (90°W), drives cyclonic trajectories through central Chile.

In the present work, we will attempt to document the SH storm tracks and wave propagation characteristics during the ENSO extremes over southern South Amer-

Corresponding author address: Dr. Silvina Solman, CIMA, Ciudad Universitaria–Pabellón 2, Piso 2, (1428) Buenos Aires, Argentina.
E-mail: solman@at.fcen.uba.ar

ica, the Drake Passage and neighboring oceans. We will include some relevant diagnostics of the mean circulation and indicators of the transient eddy activity. Baroclinic waves in the SH storm tracks tend to be organized in localized downstream-developing wave packets. Berbery and Vera (1996) used 6 yr of European Centre for Medium-Range Weather Forecasts (ECMWF) daily analyses to document the horizontal structure and evolution of wintertime baroclinic waves in the SH, based on one-point lag-correlation analysis. They showed that during austral winters, synoptic-scale waves propagate along both the subtropical and subpolar jet axes over the Pacific Ocean. They also noted that, especially along the subtropical branch of the westerlies, waves evolve as centers decaying upstream and growing downstream of the wave packet, suggesting that downstream development contributes to the synoptic-scale waves in the SH storm track. Chang and Yu (1999) and Chang (1999) studied the basic characteristics of wave packets in the upper troposphere for both hemispheres for winter and summer, mainly through examination of time-lagged correlation maps of the unfiltered meridional component of the wind. In Chang (1999), it was found that the main waveguide splits in two around 70°E during the SH winter, with the more coherent branch deviating equatorward to join up with the subtropical waveguide over the Pacific and a secondary branch spiraling poleward along with the subpolar jet and storm track maxima. He also showed, based on results from experiments using an idealized model, that coherence of wave packets depends not only on the baroclinicity of the large scale flow, but also on the intensity of the Hadley circulation, which acts to tighten the upper-tropospheric potential vorticity gradient. It is worth noting that the Hadley circulation is a primary component affected during the ENSO cycle.

The large interannual variability of the synoptic activity over the Southern Ocean has been known for many years and was noted, for example, by Taljaard (1965) and Carleton (1979). However, the interannual variability of SH storm tracks associated with warm and cold phases of the ENSO cycle are still for the most part unknown. Numerous authors described ENSO teleconnections over parts of the SH (e.g., van Loon and Madden 1981; Mo and White 1985; Karoly 1989; Lau et al. 1994; Mo and Higgins 1998) and Antarctica (e.g., Smith and Stearns 1993; Simmonds and Jacka 1995; Gloersen 1995; Carleton 1988). Held et al. (1989) suggested that extratropical eddies can be organized by tropical SST anomalies and that a tropically forced wave train of only modest amplitude may be sufficient to affect the storm track. They proposed that the extratropical atmosphere feels the impact of tropical heating indirectly through modification of the transient eddy forcing term by such heating. They also noted that the transient forcing could be at least partly associated with variations of the preferred trajectory of synoptic-scale midlatitude disturbances accompanying the perturbed extratropical wave train. Sinclair et al. (1997) analyzed the response of cyclone activity in the SH to ENSO variability, by determining the frequency of individual weather systems. They found that during El Niño (EN) winters, increased cyclone activity occurs in a band spiraling southeastward from the subtropical Pacific Ocean toward South America, while during La Niña (LN) winters, the patterns are almost reversed. Atmospheric circulation and sea surface temperature anomalies in the western South Atlantic Ocean appear to be linked to ENSO by mechanisms that remain unknown. Venegas et al. (1997) found three leading modes of variability of the atmosphere–ocean coupled system over the South Atlantic Ocean, one of them associated with ENSO timescales (the other two modes are associated with interdecadal variability).

Our aim is to document and characterize the interannual variations in transient behavior over the eastern Pacific Ocean–South America–Atlantic Ocean sector during the austral winter, as revealed by time series of available hemispheric gridded analyses extending over 39 yr. In particular, the main focus is to characterize the storm track and the interaction of eddies with the large-scale geopotential height anomalies for both phases of the ENSO cycle over the South American sector. In order to describe the properties of the waves and wave packet propagation we make use of time-lagged one-point correlation analysis based on reference time series for selected grid points. The data used and the methodology are described in next section. Some relevant large-scale anomalous patterns associated to ENSO-related interannual variability are discussed in section 3. The differential characteristics of waves and wave packet propagation for the extreme phases of ENSO cycle are presented in section 4. We conclude with some final remarks in section 5.

2. Data and methodology

The data used in this study comprise 39 yr (1960–1998) of twice-daily (0000 UTC and 1200 UTC) gridded analysis from the National Center for Environmental Prediction (NCEP) reanalysis database (Kalnay et al. 1996) on 2.5° latitude by 2.5° longitude grid. They represent one of the most complete, physically consistent atmospheric datasets available. They have been used for examining synoptic-scale activity in the SH in previous studies, such as Simmonds and Keay (2000a,b) who analyzed cyclone behavior and its long-term variability in the SH, and Renwick and Revell (1999), who linked the occurrence of blocking over the Southeastern Pacific Ocean to the propagation of Rossby waves forced by tropical convection. Full details of the NCEP–National Center for Atmospheric Research (NCAR) project and the dataset are given in Kalnay et al. (1996) and discussions about its quality over the SH can be found in Garreaud and Battisti (1999), Simmonds and Keay (2000a), Renwick and Revell (1999) and Kistler et al.

(2001). It should be noted that, though the reanalyses data assimilation system was maintained fixed, it could be affected by changes in the observing system, particularly due to the lack of satellite data over the Southern Ocean prior to 1979 (see below in this section).

The 300-hPa meridional wind velocity was chosen to represent high-frequency perturbations and to analyze the evolution of synoptic-scale wave packets. It has been shown that the meridional velocity in the middle latitude upper troposphere is dominated by zonal wavenumbers 5–7, which represent typically the scale of baroclinic waves (Trenberth 1981). The perturbation of the meridional wind is defined here by removing the monthly mean for each year, which filters out the interannual variability from the time series. No further filtering was necessary to capture the temporal evolution and propagation characteristics of wave packets (Chang 1993; Berbery and Vera 1996). The SH winter season is defined here as the period from 1 June to 31 August.

The standard deviation of the meridional wind perturbation is used to identify regions of enhanced high-frequency variability or storm tracks. The maxima are coincident with the regions where developing and mature synoptic-scale fluctuations occur most frequently. This measure also captures the regions where the high-frequency disturbances attain larger amplitudes. In this paper we will focus on the wave propagation characteristics in the upper troposphere, where the storm track attains its larger amplitude.

In order to analyze the response of high-frequency variability to ENSO, monthly mean sea surface temperature anomalies in the El Niño-3 region of the NCEP reanalysis data set are also used in this study for the same time period, and composite fields have been constructed for both extreme phases of ENSO. Because SST anomalies time series shows a trend for stronger warm events in the last two decades, the time series has been detrended using a 9-yr running mean filter (Fedorov and Philander 2000). A 5-month running mean filter was then applied to the monthly SST anomalies in order to smooth out intraseasonal variations (Trenberth 1997). Months having SST anomalies larger than 0.7°C (El Niño or warm phase) and less than −0.6°C (La Niña or cold phase) were composed, with each subset comprising 22 months. This threshold to define warm and cold phases of ENSO, respectively, is determined in order to have the same number of analysis for both phases of ENSO involved in the calculation of the composites to make them comparable and to capture only extreme events. Besides, the assignments of events agree with the list of El Niño and La Niña events in Trenberth (1997).

The main analysis tool to examine the characteristics of the waves and their preferred propagation paths is based on one-point lag-correlation analysis. This analysis is useful to study the spatial and temporal evolution of mean baroclinic waves and, particularly, the characteristics of wave packets. This technique has been used by other authors, such as Berbery and Vera (1996) and Chang (1999) for the SH. A slightly different approach was used by Lim and Wallace (1991) and Chang (1993) to study the structure of baroclinic waves in the Northern Hemisphere winter, in which regression maps were analyzed. The advantage of regression analysis is that the regression coefficients carry the units of the regressed variable, and they may be interpreted as the amplitude of the disturbances in each grid point that are observed in association with a positive perturbation in the reference variable with an amplitude of one standard deviation. We performed both analyses but we chose to display correlation maps in which statistical tests of significance of the inferred results were performed.

The statistical significance of the correlation has been assessed using a Fisher test (F-test) taking into account that for twice-daily analyses only 1 in 10 independent analyses should be taken into account (considering the effective time between independent samples on a synoptic timescale to be 5 days). Assuming 120 degrees of freedom (since each subset of analyses for warm and cold composites, respectively, involve 1200 analyses), correlations of magnitude 0.15 or larger are significantly different from zero at 5% level.

As mentioned before, the lack of operational satellite information prior to 1979 could affect the homogeneity of the analysis. In order to test the stability of the patterns, we split the dataset in halves (1960–78 and 1979–98) and computed the two more important diagnostics related to storm tracks in this paper: variance of meridional component of the wind and correlation maps. First, we applied the F-test for significantly different variances and we found no statistical significant differences between both periods at a confident level of 5%. We then computed the correlation maps for selected base points and evaluated the significance of the difference between the two calculated correlation coefficients using the Fisher's *z*-transformation to each computed correlation coefficient. No statistically significant difference was found at a 5% level of confidence for all the base points analyzed. In light of these results we decided that the period 1960–98 is an appropriate dataset for our purpose.

The statistical significance of the differences between warm and cold composites were also assessed. A Fisher test for significantly different variances was performed assuming 120 degrees of freedom and a confidence level of 10% to support the discussion about the difference in the storm tracks. For the correlation maps, differences between warm and cold composites were assessed using Fisher's *z*-transformation to test whether one correlation differs significantly from another. Statistically significant differences were considered at a 10% level of confidence.

3. Interannual variability of the mean circulation

In this section we examine the mean structure of the warm and cold events signals for the southern extra-

tropics. In general, the changes in the mean flow are largely consistent with previous work (Karoly 1989; Kiladis and Mo 1998; Garreaud and Battisti 1999), so we will concentrate only on those features referred to later. A close connection exists between the variability of the planetary wave structure and the location or intensity of the storm tracks according to observational evidence presented by Lau (1988), Metz (1989), and others. The higher frequency extratropical transients, which owe their existence to the baroclinic instability, tend to reinforce any preexistent perturbation in the background flow mainly through eddy transports of vorticity in the upper troposphere. Therefore the anomalies in the large-scale flow must be related with zones of enhanced baroclinicity. The Eady growth rate parameter [$\sigma = 0.31\ (f/N)\ |\mathbf{V}_z|$, using standard notation; Fig. 1] is commonly used for diagnosing the baroclinicity of the mean flow. In general, the characteristics of the upper-level winds (not shown here) are reflected in the structure of σ and the changes in the mean baroclinicity are consistent with the zonal wind and geopotential height anomalies. Positive (negative) anomalies (see Fig. 1c) would lead to preferred sites for the genesis and intensification of fast-moving disturbances during warm (cold) events. During warm events, the axis of the positive anomalies extends from the tropical western Pacific Ocean eastward spiralling in toward the pole. The axis of maximum σ is stronger during EN (Fig. 1a) and shifts equatorward over the subtropical Pacific, in agreement with an anomalously low pressure extending along about 35°S over the central Pacific Ocean (as shown, e.g., in Garreaud and Battisti 1999, their Fig. 3b). Another well-known feature during warm events is the positive anomaly of geopotential height over the Bellingshausen Sea, consistent with a predisposition toward blocking episodes southwest of the southern tip of South America during EN years (e.g., Rutllant and Fuenzalida 1991; Renwick 1998). The Bellingshausen Sea coastal region, where the relatively temperate, maritime air masses meet the cold, continental air from Antarctica is consistently an area of considerable thermal contrast during EN winters. Over South America, a reversal between warm and cold events is manifested in the baroclinicity near 35°S (enhanced σ during EN). Over the Atlantic and Indian Oceans, the axes of maximum σ are intensified and shift poleward during EN. It is worth noting that in general the anomalies in the mean circulation are stronger and more stable over the Pacific than over the Atlantic Ocean.

Figures 2 and 3 show a measure of the high-frequency variability at 850 and 300 hPa. It is interesting to note that all the regions with enhanced activity at 300 hPa are located just downstream of positive baroclinicity maxima. A significant difference in the high frequency activity between warm and cold events is manifested especially in the Pacific Ocean sector (see Figs. 2c and 3c). The blocking of the westerly flow and the weakening of the subtropical high indicates that there is an equatorward shift of the storm track axis over the central Pacific Ocean during EN winters. This result, particularly evident at 850 hPa, is consistent with the findings of Sinclair et al. (1997). However, in the upper troposphere the standard deviation is weaker over the major part of the Pacific Ocean, except south of New Zealand and around 20°S near South America. Consistently, over the Pacific Ocean and during EN winters, the transient baroclinic eddies produce a weaker convergence of westerly momentum in the upper troposphere near 50°–60°S and a weaker poleward eddy heat flux in the lower troposphere, and vice versa during LN winters (not shown here). The Antarctic Peninsula—a 2-km-high topographic barrier—is a major obstacle to the progression eastward of depressions and causes many systems to stagnate in the eastern Bellingshausen Sea. Variations in cyclone activity appear related to the strength of the westerly circulation, which actively enhances lee cyclogenesis near the Antarctic Peninsula (Mayes 1985). During the warm phase of ENSO, the 850-hPa eddy activity is weaker over the Bellingshausen–Amundsen Seas and slightly stronger over the western Weddell Sea, consistent with the height anomaly pattern.

In order to guarantee that the changes between EN and LN are dominated by baroclinic eddies, we performed the same analysis utilizing a bandpass filter that retains only the synoptic-scale baroclinic waves. As shown by Simmons and Hoskins (1978) waves with periods up to 10 days have a variance related to baroclinic instability. The bandpass filter applied here (Murakami 1979) covers a range from about 3–9 days with a center at day 6 (as previously used in Menéndez et al. 1999). The differences in the standard deviation between EN and LN using filtered data (Fig. 4) exhibit very similar patterns compared with the unfiltered data (note that the statistical significance of the differences is, in general, larger especially in the southern Pacific Ocean). We can conclude that the changes discussed in the previous paragraph are due to synoptic-scale waves. However, as time filtering of the data distorts the temporal evolution of the waves (Chang 1993; Berbery and Vera 1996), in what follows correlation maps are calculated using unfiltered data.

4. Characteristics of the waves and wave-packet propagation for warm and cold phases of ENSO

A complete picture of the large-scale circulation that could arise from the high-frequency forcing of the storm track has been given in Orlanski (1998). That paper demonstrates that the pattern of the forcing by the high-frequency eddies along the storm track is highly correlated with the stationary circulation, and the forcing itself is primarily responsible for the location of the trough–ridge system associated with the stationary flow. Moreover, by this argument the monthly variability and the interannual variability of the wintertime storm track

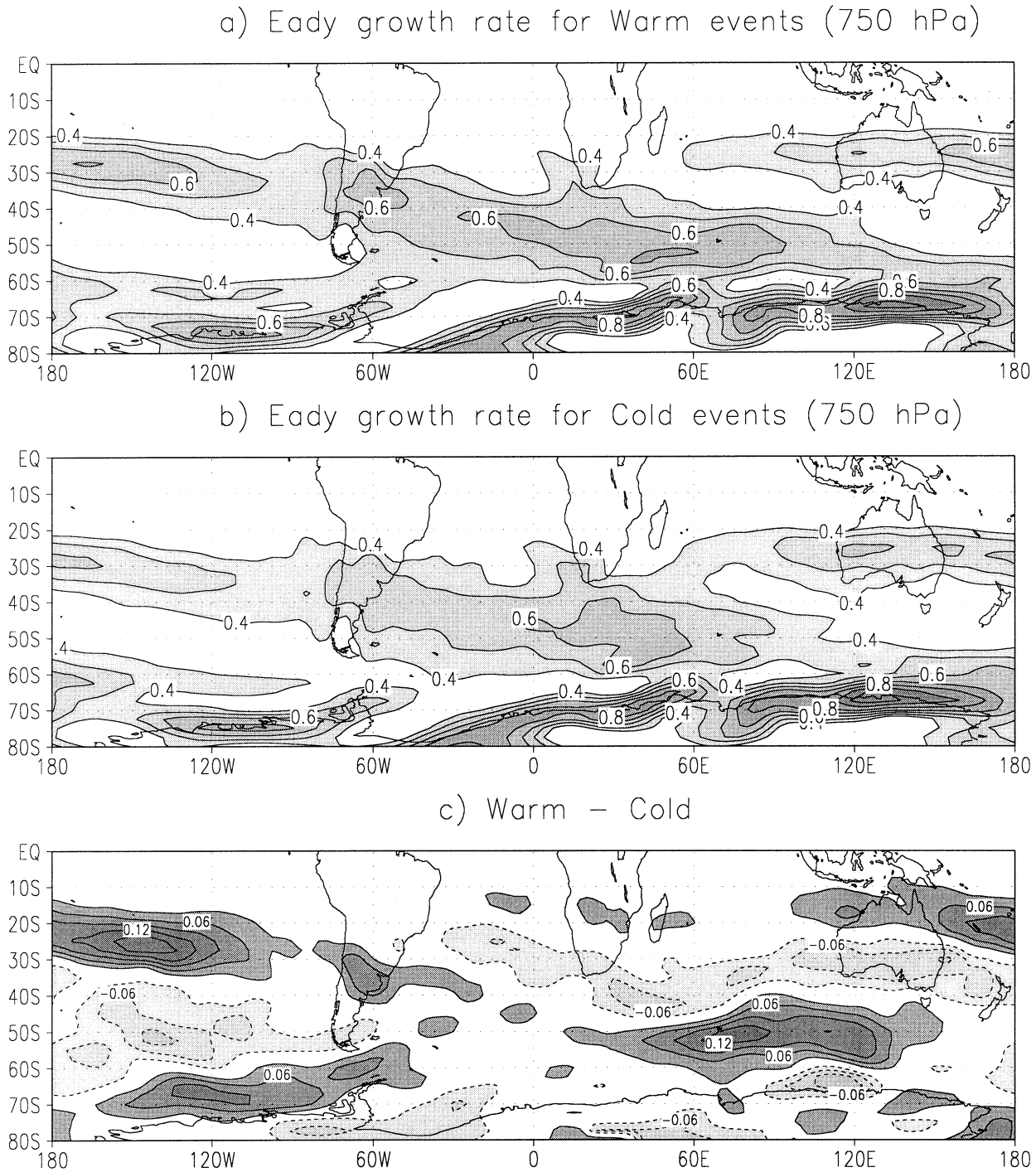

FIG. 1. Mean Eady growth rate computed for the 850–500-hPa layer for (a) warm events and (b) cold events. Contour interval is 0.1 day^{-1}, minimum contour is 0.4 day^{-1}. (c) Difference between warm and cold events. Contour interval is 0.03 day^{-1}. Light shading is for negative values and dark shading is for positive values. Zero contour is omitted.

in the North Pacific Ocean are explained. In our case, the presence of an anomalous blocking high in the southeastern Pacific Ocean during warm events is consistent with the decrease in the eddy activity at high and low levels in that region. Though the analysis of the high-frequency forcing in supporting the large-scale circulation is beyond the scope of this study, we will focus on the characteristics of high-frequency disturbances, their evolution and propagation, that determine the shape and intensity of the storm track during the extreme

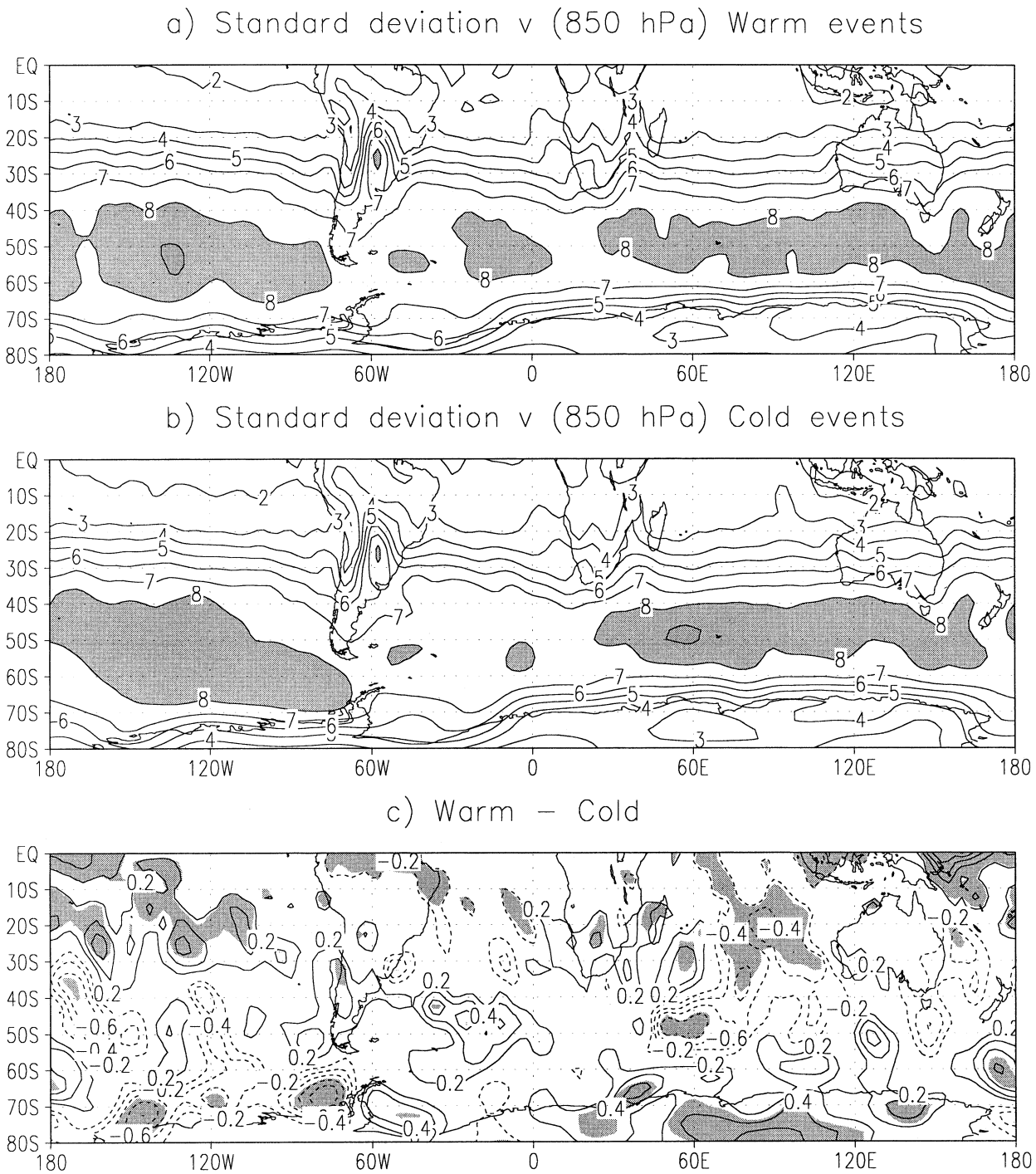

FIG. 2. Standard deviation of the meridional wind anomaly at 850 hPa for (a) warm events and (b) cold events. Contour interval is 1 m s^{-1}. Regions with std dev greater than 8 m s^{-1} are shaded. (c) Difference between warm and cold events. Contour interval is 0.2 m s^{-1}. Zero contour is omitted. Shading denotes regions over which the differences are significant at a 10% confidence level.

phases of ENSO and the consistency with the anomaly pattern of geopotential heights.

The basic characteristics of upper-level waves and wave-packet propagation for the Southern Hemisphere winter have been extensively examined by Berbery and Vera (1996) and Chang (1999). In this section we will discuss the differences in wave propagation characteristics for both extremes of the ENSO cycle, by analyzing sequences of time-lagged correlation maps computed at some strategic locations. We

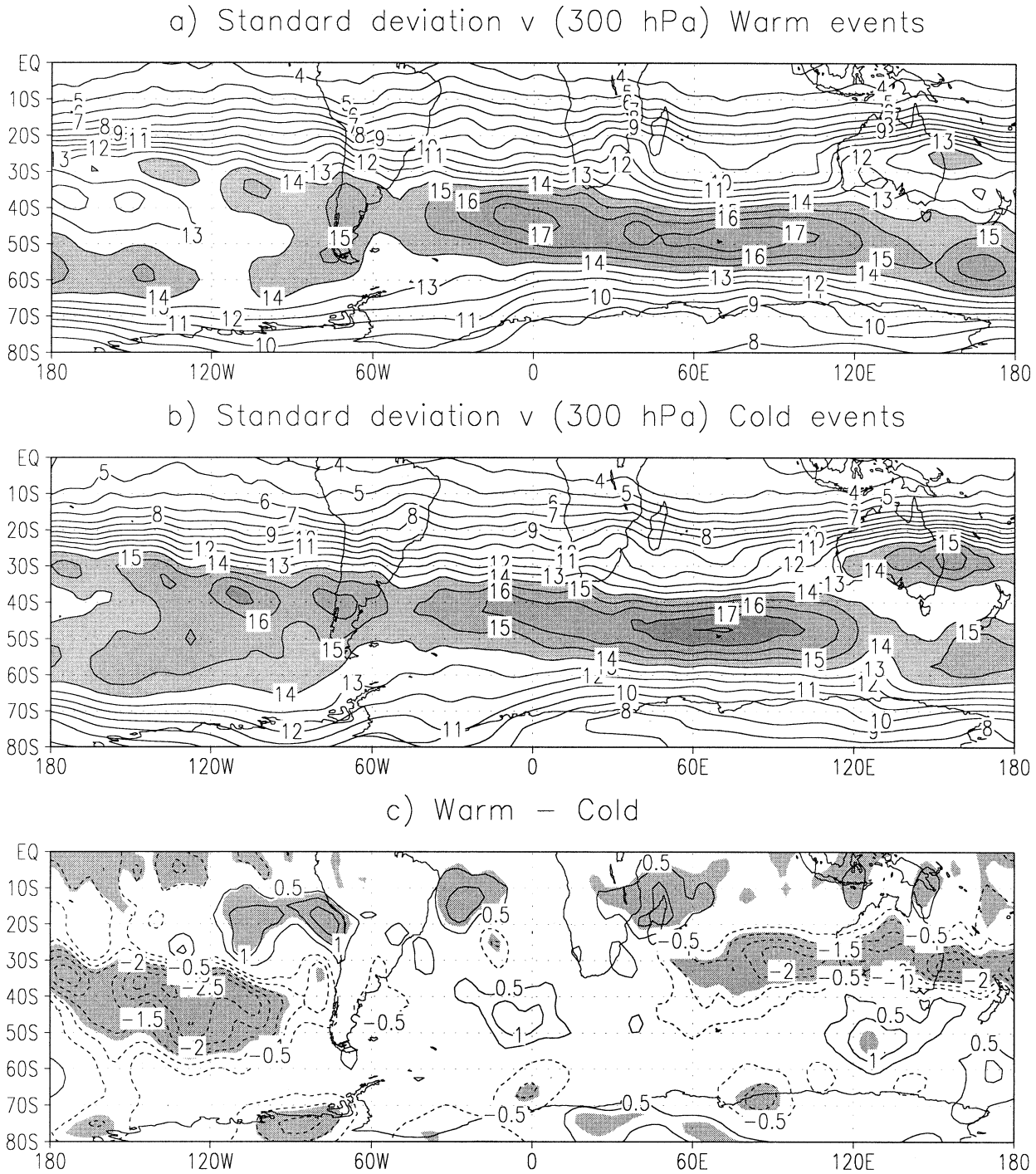

FIG. 3. Standard deviation of the meridional wind anomaly at 300 hPa for (a) warm events and (b) cold events. Contour interval is 1 m s^{-1}. Regions with std dev greater than 14 m s^{-1} are shaded. (c) Difference between warm and cold events. Contour interval is 0.5 m s^{-1}. Zero contour is omitted. Shading denotes regions over which the differences are significant at a 10% confidence level.

have computed one-point lagged correlation and regression maps for base points at 300 hPa each 30° longitude along the main body of the storm track with the time series at each grid point on 300 hPa in order to have a picture of the horizontal structure of the disturbances. Correlation and regression maps at 850–300 hPa with base points at 300–850 hPa were also computed to have an indication of the vertical tilt of the disturbances. As we are particularly interested in waves that develop near southern South America, the

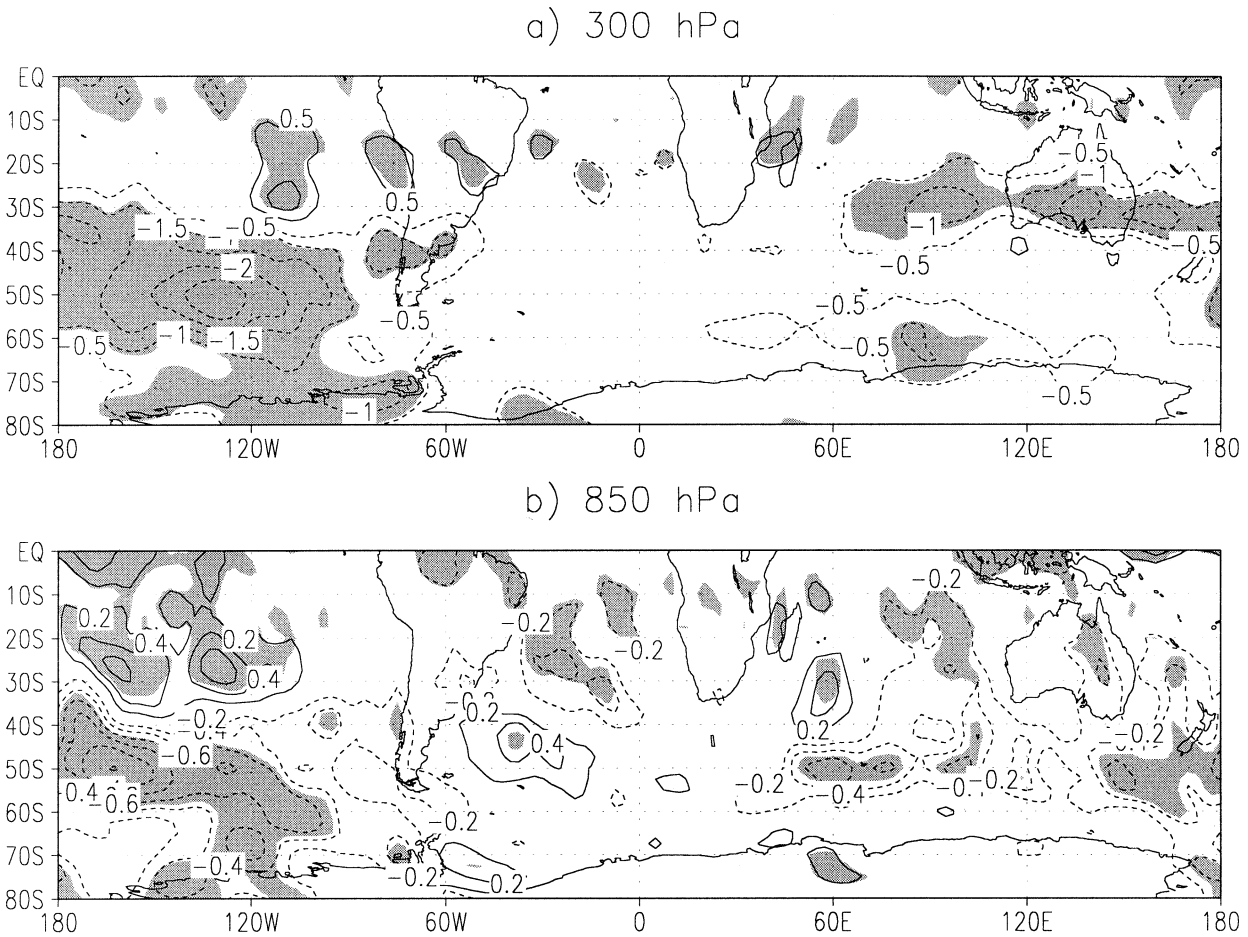

FIG. 4. Differences between warm and cold events of the bandpass-filtered (3–9 days) std dev of the meridional wind for (a) 300 hPa and (b) 850 hPa. Contour interval is (a) 0.5 m s^{-1} and (b) 0.2 m s^{-1}. Zero contour is omitted. Shading denotes regions over which the differences are significant at a 10% confidence level.

analysis has been concentrated on waves that evolve within the subtropical and subpolar branches of the Pacific Ocean storm track and the entrance of the Atlantic Ocean storm track. Base points at 60°S, 180°; 35°S, 90°W, and 40°S, 30°W are analyzed in Figs. 5 to 8.

We will examine first the correlation maps from lag day −2 to lag day +2 for the base point located at 60°S, 180°, within the polar branch of the Pacific Ocean storm track. As has been pointed out before, this region shows a strong signal of interannual variability in the upper- and lower-level storm tracks, Eady growth rate, and geopotential height field. Figure 5 shows the correlation maps at 300 hPa, for warm (left) and cold (right) events. At lag 0 the correlation maps typically show a wave train extending through the southern Pacific Ocean, with several positive and negative phases. The sequence of time-lagged correlation maps shows upstream centers decaying while new centers are growing downstream, typical of downstream development. Using these maps we can also estimate the wavelength and phase speed of the waves in the way described in Chang and Yu (1999). When we examine the upstream direction (lags −2 and −1) we can see that both extremes of ENSO waves emanate from the main body of the Atlantic–Indian Ocean storm track and propagate toward the polar branch of the Pacific Ocean storm track. The extension of the wave packet is greater for LN events consistent with weaker baroclinicity. Nevertheless, greater magnitudes of the regressions (not shown) are found in the Australian sector during warm events, consistent with enhanced eddy activity downstream of the maximum positive baroclinicity anomaly. In the downstream direction (positive lags) the waves acquire a NW–SE tilt. For cold events they tend to propagate in the NE direction downstream from the positive height anomaly centered at 35°S, 150°W with a weaker branch toward the east, and exhibit larger meridional extent over the eastern Pacific Ocean. In contrast, the propagation for warm events is entirely toward the east. For the warm composite, the wavelength is significantly larger than for the cold composite (4100 km and 3800 km, respectively). Although the blocking anticyclone prevents the propagation of waves in the southeastern Pacific Ocean

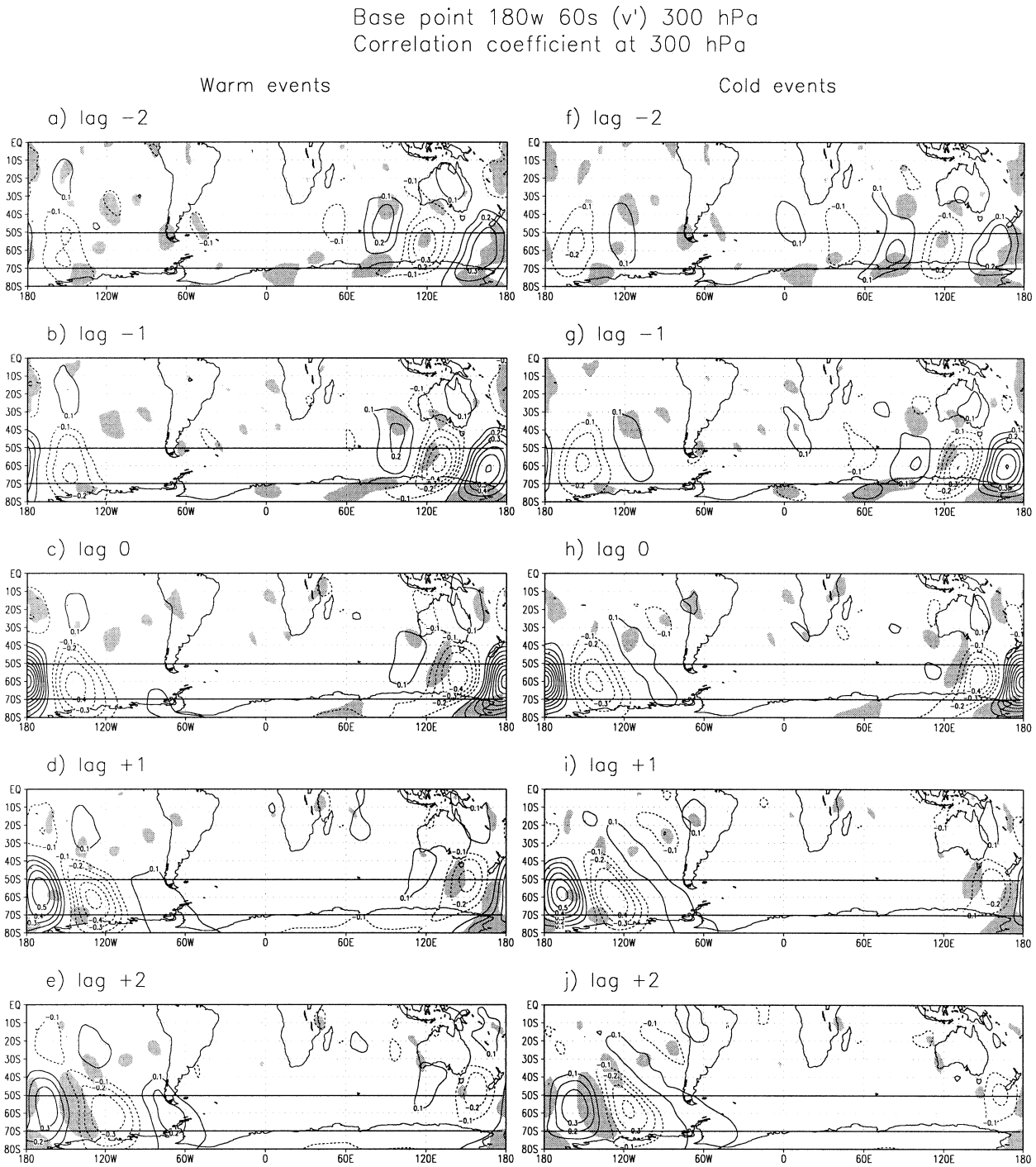

FIG. 5. One-point lag correlation maps for v' at 300 hPa for the base point at 60°S, 180° at 300 hPa, from lag day −2 to lag day +2. (a)–(e) warm events; (f)–(j) cold events. Contour interval is 0.1. Gray lines along 50° and 70°S have been drawn for reference. Shading denotes regions over which correlations for EN and LN are significantly different at a 10% confidence level.

during warm events, the enhanced baroclinicity around 120°W constitutes a source of energy that contributes to maintain the eddy activity in that region.

By examining the regression maps (not shown) we found that for warm events the disturbances have larger amplitude than for cold events over the eastern Indian Ocean and western Pacific Ocean, consistent with enhanced baroclinicity over that area. At lag +2 enhanced eddy activity is apparent over the Drake Passage region for warm events downstream from the blocking anti-

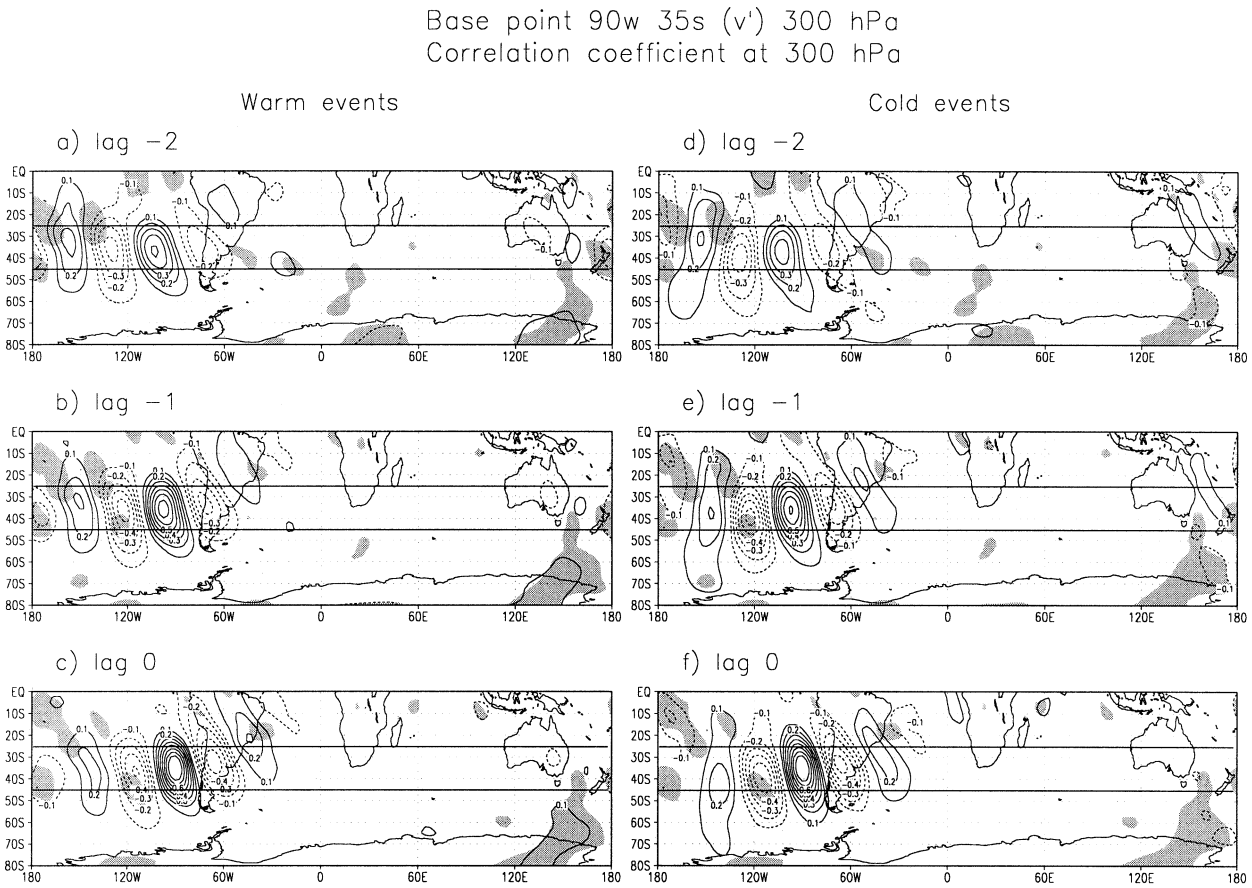

FIG. 6. Same as Fig. 5 but for the base point at 35°S, 90°W, from lag day −2 to lag day 0. (a)–(c) warm events; (d)–(f) cold events. Gray lines along 25° and 45°S have been drawn for reference.

cyclone, and waves tend to have a barotropic equivalent structure.

Over the subtropical Pacific Ocean large-scale circulation patterns show a strong ENSO-related signal, and hence, the synoptic-scale activity, which develops within such different characteristic mean fields for both extremes of ENSO, will show different characteristics too. In Figs. 2 and 3, the storm tracks for warm and cold phases of ENSO were analyzed and it was pointed out that the subtropical Pacific Ocean area was characterized as a region with strong interannual variability. To investigate further the difference in eddy activity for the extreme phases of ENSO over this region, we will examine the correlation maps for a base point located at 35°S, 90°W (Fig. 6). Waves propagating within the subtropical branch of the Pacific Ocean storm track have

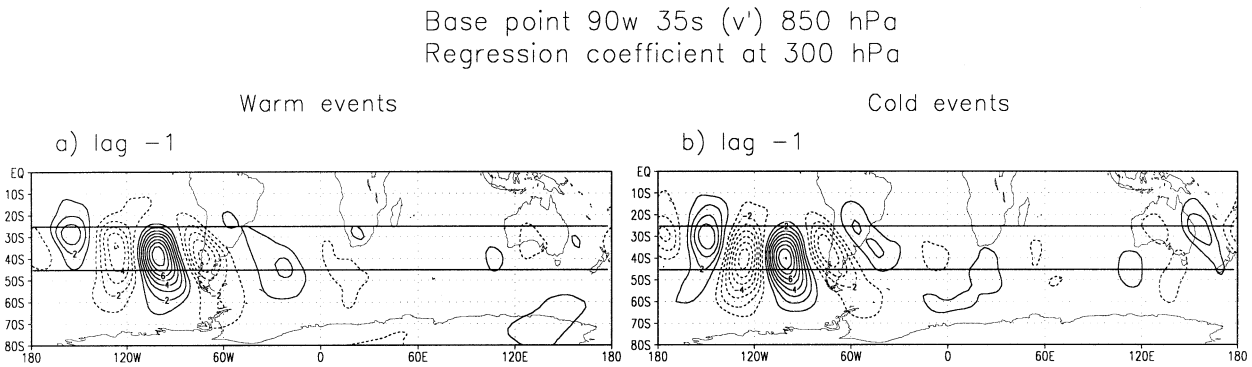

FIG. 7. One-point lag regression maps for v' at 300 hPa for the base point at 35°S, 90°W at 850 hPa for lag day −1 for (a) warm events and (b) cold events. Contour interval is 1 m s^{-1}.

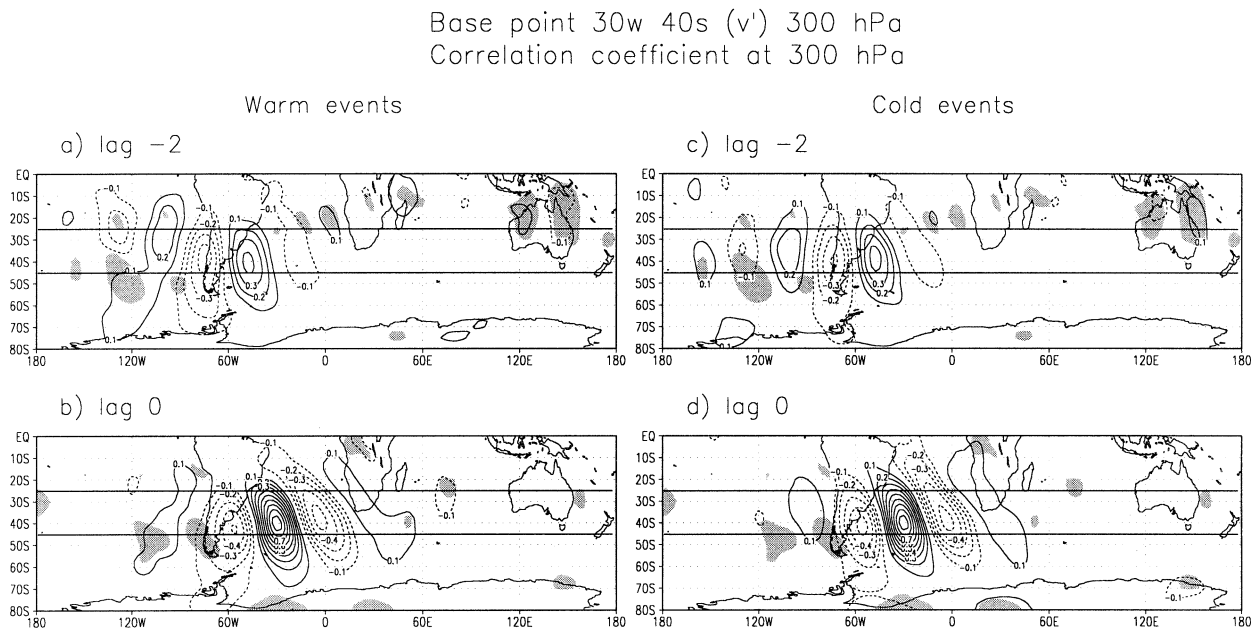

FIG. 8. Same as Fig. 5 but for the base point at 40°S, 30°W and lag day −2 and 0 (a)–(b) warm events; (c)–(d) cold events. Gray lines along 30° and 50°S have been drawn for reference.

a typical wavelength of the order of 4500 km and a more baroclinic structure compared with those propagating into the subpolar branch. Also, the wave packet is more coherent than waves propagating along the subpolar branch of the jet stream, as noted previously by Berbery and Vera (1996) and Chang (1999). By examining the upstream direction we can see that for cold events, waves emanate from eastern Australia while for warm events the propagation comes from higher latitudes. However, as waves propagate through the central and eastern Pacific Ocean, the wave train seems to propagate along a latitude circle between 30° and 35°S during warm events, while for cold events there is a tendency of the waves to propagate along a more southern path. This agrees with the latitudinal displacement of the subtropical jet and the maximum baroclinicity area. In addition, an examination of the regression maps (not shown) evidenced that the amplitude of the disturbances at 300 hPa is smaller during the warm phase, consistent with a weaker upper-level storm track. This weakening of the eddy activity in the region of the subtropical jet at upper levels deserves a closer examination. In Figs. 1, 2, and 3 it was noted the consistency between the distribution of eddy activity at lower and upper levels and the baroclinic zone, the latter slightly upstream of the storm track maximum. Following Hoskins (1983), Chang and Orlanski (1993) and Orlanski and Gross (2000), the eddies grow initially by baroclinic processes and, as they mature they grow deeper by fluxing energy upward and downstream, extending the storm track well downstream of the region of maximum baroclinicity. For EN, larger baroclinicity over the subtropical Pacific Ocean favors the generation of synoptic-scale waves, as found by Sinclair et al. 1997. However, the intensified upper-level subtropical jet contributes to a stronger advection of the waves. This reduces the residence time over the enhanced baroclinic zone and waves attain smaller amplitude (Vera 2002). Moreover, a larger baroclinicity source conduces to a more rapid growth and decay of the eddies (correlation maps at 850 hPa—not shown—evidence that for warm events the westward tilt of the waves with height is larger than for cold events). Due to the fact that eddies grow rapidly and decay before radiating energy upward, eddy activity at upper levels is reduced (as was shown in Fig. 3). Evidence of that process is the larger meridional extension of the waves for cold events, associated with the enhanced ridge over the central Pacific Ocean (Fig. 6). On the contrary, for warm events the meridional extension of the waves is more confined, indicating that waves do not grow enough to radiate energy to upper levels (Orlanski 1998). In order to further support this statement an additional diagnosis was performed by regressing v' at 300 hPa with the base point at 850 hPa (Fig. 7), to show the relative amplitude of wave disturbances at different altitudes. Over the region of the subtropical jet the amplitude of the centers is smaller for the warm events compared to the cold events, indicating that the disturbances are more vertically confined for EN. This corroborates that the upward radiation of energy is less effective during warm events (i.e., the waves are shallower).

To complete the picture, we finally examine the correlation maps for a base point located at 40°S, 30°W, near the storm track entrance region on the South Atlantic Ocean, which is shown in Fig. 8. Looking toward

the upstream direction, upper-level disturbances propagate mainly from the subtropical branch of the Pacific Ocean storm track. In agreement with Fig. 6, waves propagate from a more northern path during warm events. During this phase of ENSO, it is also evident that waves have propagated from the subpolar branch of the Pacific Ocean storm track too. According to Chang (1999), wave propagation over the high-latitude branch of the storm track apparently stops near 0°, being the main source of waves the subtropical branch of the storm track. Nevertheless, as is suggested by our figure, during warm events weak, though significant, correlations are found upstream of the base point over the mid- to high latitudes of the Pacific Ocean, not evident during cold events. Thus for EN, waves over the western Atlantic Ocean are partially fed by disturbances travelling along the subpolar branch of the Pacific Ocean storm track.

5. Summary and conclusions

The ENSO-related variability of winter storm tracks over the southeastern Pacific Ocean–South America–southwestern Atlantic Ocean sector has been addressed with the objective of analyzing the differential behavior of synoptic-scale waves that affect the region. We have focused on the predominant large-scale circulation anomalies during the warm and cold phases of ENSO and the structure and propagation characteristics of upper troposphere synoptic-scale disturbances for both extremes of the ENSO cycle. A correlation analysis was applied to winter anomalies of the meridional wind at 300 hPa for the period 1960–98 using the NCEP reanalysis data set to evaluate the structure and propagation characteristics of synoptic-scale waves. The dataset has been stratified based on El Niño-3 anomalies to identify warm and cold phases of the ENSO cycle.

From examination of wave packet propagation based on correlation and regression maps we can summarize the behavior of high-frequency disturbances in the South Pacific–South Atlantic Ocean sector for extreme phases of the ENSO cycle. During warm events, disturbances developing within the main body of the storm track over the Atlantic and Indian Oceans propagate preferentially towards the subpolar branch of the storm track near Australia, manifested through higher magnitudes of the correlations. As waves approach the blocking high over the southeastern Pacific Ocean, which tends to block their propagation, eddies develop over a region of enhanced baroclinicity near the Antarctic coast that contributes to maintain the eddy activity. Downstream of the blocking anticyclone, the wave-packet propagates toward the NE into the Atlantic Ocean and waves develop further in the downstream direction. Along the subtropical branch of the Pacific Ocean storm track, the wave train seems to propagate along a northern path, compared with the cold events composite, consistent with the equatorward shift of the subtropical westerly jet and maximum baroclinicity areas. As waves develop over a region of strong low-level baroclinicity and strong upper-levels winds, their life cycle is more explosive and they do not grow enough to radiate energy upward; as a consequence, they do not reach a robust development. This is translated in large eddy activity at lower levels but weak eddy activity at upper levels. As the wave packets propagate downstream of the Andes, it splits into two branches with the more coherent one propagating further across the Atlantic–Indian Ocean storm track.

During cold events, wave packets emanating from the Atlantic–Indian Ocean storm track propagate more coherently towards the subtropical branch of the storm track over the South Pacific Ocean. The propagation along the subpolar axis of the westerly jet over the South Pacific Ocean is, in part, deflected to the NE due to the intensification of the ridge in the central Pacific Ocean. Along the subtropical branch of the storm track over the Pacific Ocean, the wave train propagation evidences a poleward deflection and waves develop over a broader area over the central Pacific Ocean. Waves attain larger amplitudes at upper levels, compared to the warm composite. It is apparent from the analysis that waves propagating through the Atlantic Ocean storm track during cold events have arisen from the subtropical branch of the Pacific Ocean storm track, but for warm events, it appears to have propagated from the subpolar branch too.

Previous studies (e.g., Garreaud and Battisti 1999) showed that tropical SST anomalies associated with ENSO can induce large-scale atmospheric circulation anomalies over large areas of the SH and, in particular, in the eastern South Pacific Ocean–South America–South Atlantic Ocean sector. Our results suggest an intimate relationship between the storm tracks and these extratropical large-scale anomalies and could be viewed as additional evidence that the Pacific Ocean–South America pattern functions as a link whereby tropical SST anomalies induce changes in the storm tracks.

Acknowledgments. The authors are particularly grateful to Dr. Isidoro Orlanski for his helpful comments and discussions on many topics of this study. We would also like to thank the anonymous reviewers who helped improve the paper. This work was supported by ANPCyT Grant 04446 and ANPCyT Grant 7-6335. NCEP–NCAR reanalysis data were provided through the NOAA Climate Diagnostics Center.

REFERENCES

Berbery, H., and C. Vera, 1996: Characteristics of the Southern Hemisphere winter storm track with filtered and unfiltered data. *J. Atmos. Sci.,* **53,** 468–481.

Carleton, A. M., 1979: A synoptic climatology of satellite-observed extratropical cyclones activity for the Southern Hemisphere winter. *Arch. Meteor. Geophys. Bioklimatol.,* **B27,** 265–279.

——, 1988: Sea–ice atmosphere signal of the Southern Oscillation in the Weddell Sea, Antarctica. *J. Climate,* **1,** 379–388.
Chang, E. K. M., 1993: Downstream development of baroclinic waves as inferred from regression analysis. *J. Atmos. Sci.,* **50,** 2038–2053.
——, 1999: Characteristics of wave packets in the upper troposphere. Part II: Seasonal and hemispheric variations. *J. Atmos. Sci.,* **56,** 1729–1747.
——, and I. Orlanski, 1993: On the dynamics of a storm track. *J. Atmos. Sci.,* **50,** 999–1015.
——, and D. B. Yu, 1999: Characteristics of wave packets in the upper troposphere. Part I: Northern Hemisphere winter. *J. Atmos. Sci.,* **56,** 1708–1728.
Fedorov, A. V., and S. G. Philander, 2000: Is El Niño changing? *Science,* **288,** 1997–2002.
Garreaud, R. D., and D. S. Battisti, 1999: Interannual (ENSO) and interdecadal (ENSO-like) variability in the Southern Hemisphere tropospheric circulation. *J. Climate,* **12,** 2113–2123.
Gloersen, P., 1995: Modulation of hemispheric sea-ice cover by ENSO events. *Nature,* **373,** 503–506.
Held, I. M., S. W. Lyons, and S. Nigam, 1989: Transients and the extratropical response to El Niño. *J. Atmos. Sci.,* **46,** 163–174.
Hoskins, B. J., 1983: Theory of transient eddies. *Large-scale Dynamical Processes in the Atmosphere,* B. H. Hoskins and P. R. Pearce, Eds., Academic Press, 397 pp.
Kalnay, E., and Coauthors, 1996: The NCEP/NCAR 40-Year Reanalysis Project. *Bull. Amer. Meteor. Soc.,* **77,** 437–471.
Karoly, D. J., 1989: Southern Hemisphere circulation features associated with El Niño–Southern Oscillation events. *J. Climate,* **2,** 1239–1251.
Kiladis, G. N., and K. C. Mo, 1998: Interannual and intraseasonal variability in the Southern Hemisphere. *Meteorology of the Southern Hemisphere, Meteor. Monogr.,* No. 27, Amer. Meteor. Soc., 307–336.
Kistler, R., and Coauthors, 2001: The NCEP–NCAR 50-Year Reanalysis: Monthly means CD-ROM and documentation. *Bull. Amer. Meteor. Soc.,* **82,** 247–267.
Lau, M. K., P. J. Sheu, and I. S. Kang, 1994: Multiscale low-frequency circulation modes in the global atmosphere. *J. Atmos. Sci.,* **51,** 2753–2770.
Lau, N. C., 1985: Modeling the seasonal dependence of the atmospheric response to observed El Niños in 1962–76. *Mon. Wea. Rev.,* **113,** 1970–1996.
——, 1988: Variability of the observed midlatitude storm tracks in relation to low-frequency changes in the circulation pattern. *J. Atmos. Sci.,* **45,** 2718–2743.
Lim, G. H., and J. M. Wallace, 1991: Structure and evolution of baroclinic waves as inferred from regression analysis. *J. Atmos. Sci.,* **48,** 1718–1732.
Mayes, P. R., 1985: Secular variations in cyclone frequencies near the Drake Passage, southwest Atlantic. *J. Geophys. Res.,* **90,** 5829–5839.
Menéndez, C. G., V. Serafini, and H. Le Treut, 1999: The storm tracks and the energy cycle of the Southern Hemisphere: Sensitivity to sea-ice boundary conditions. *Ann. Geophys.,* **17,** 1478–1492.
Metz, W., 1989: Low-frequency anomalies of atmospheric flow and effects of cyclone-scale eddies: A canonical correlation analysis. *J. Atmos. Sci.,* **46,** 1026–1041.
Mo, K. C., and G. H. White, 1985: Teleconnections in the Southern Hemisphere. *Mon. Wea. Rev.,* **113,** 22–37.
——, and R. W. Higgins, 1998: The Pacific South America modes and tropical convection during the Southern Hemisphere winter. *Mon. Wea. Rev.,* **126,** 1581–1595.
Murakami, M., 1979: Large-scale aspects of deep convective activity over the GATE area. *Mon. Wea. Rev.,* **107,** 994–1013.
Orlanski, I., 1998: Poleward deflection of storm tracks. *J. Atmos. Sci.,* **55,** 2577–2599.
——, and B. Gross, 2000: The life cycle of baroclinic eddies in a storm track environment. *J. Atmos. Sci.,* **57,** 3498–3513.
Renwick, J. A., 1998: ENSO-related variability in the frequency of South Pacific blocking. *Mon. Wea. Rev.,* **126,** 3117–3123.
——, and M. J. Revell, 1999: Blocking over the South Pacific and Rossby wave propagation. *Mon. Wea. Rev.,* **127,** 2233–2247.
Rutllant, J., and H. Fuenzalida, 1991: Synoptic aspects of the central Chile rainfall variability associated with the Southern Oscillation. *Int. J. Climatol.,* **11,** 63–76.
Simmonds, I., and T. H. Jacka, 1995: Relationships between the interannual variability of Antarctic sea ice and the Southern Oscillation. *J. Climate,* **8,** 637–647.
——, and K. Keay, 2000a: Mean Southern Hemisphere extratropical cyclone behavior in the 40-Year NCEP–NCAR Reanalysis. *J. Climate,* **13,** 873–885.
——, and ——, 2000b: Variability of Southern Hemisphere extratropical cyclone behavior, 1958–97. *J. Climate,* **13,** 550–561.
Simmons, A. J., and B. J. Hoskins, 1978: The life cycles of some nonlinear baroclinic waves. *J. Atmos. Sci.,* **35,** 414–432.
Sinclair, M. R., J. A. Renwick, and J. W. Kidson, 1997: Low-frequency variability of Southern Hemisphere sea level pressure and weather system activity. *Mon. Wea. Rev.,* **125,** 2531–2543.
Smith, S. R., and C. R. Stearns, 1993: Antarctic pressure and temperature anomalies surrounding the minimum in the Southern Oscillation index. *J. Geophys. Res.,* **98** (D7), 13 071–13 083.
Taljaard, J. J., 1965: Cyclogenesis, cyclones and anticyclones in the Southern Hemisphere during the period June to December 1958. *Notos,* **14,** 73–84.
Trenberth, K. E., 1981: Observed Southern Hemisphere eddy statistics at 500 mb: Frequency and spatial dependence. *J. Atmos. Sci.,* **38,** 2159–2178.
——, 1997: The definition of El Niño. *Bull. Amer. Meteor. Soc.,* **78,** 2771–2777.
van Loon, H., and R. A. Madden, 1981: The Southern Oscillation. Part I: Global associations with pressure and temperature in northern winter. *Mon. Wea. Rev.,* **109,** 1150–1162.
Venegas, S. A., L. A. Mysak, and D. N. Straub, 1997: Atmosphere–ocean coupled variability in the South Atlantic. *J. Climate,* **10,** 2904–2920.
Vera, C. S., 2002: Interannual and interdecadal variability of atmospheric synoptic-scale activity in the Southern Hemisphere. *J. Geophys. Res.,* in press.